Effect of cooling rate on the microstructure of crystallizing LCATS-1 lunar regolith simulant. Anis Parsapoor and Alan Whittington[1], A. Majlesi[2], O. Giberga[3], R. Wells[4], S. Ximenes[4], [1]Department of Earth and Planetary Sciences, [2]Department of Civil and Environmental Engineering, [3]College of Liberal and Fine Arts, The University of Texas at San Antonio, One UTSA Circle, San Antonio TX 78249, [4]Astroport Space Technologies, Inc., 110 E. Houston Street, 7th Floor, San Antonio, TX 78205. Email: anis.parsapoor@utsa.edu

Introduction: The lunar regolith is an important potential resource for in-situ resource utilization (ISRU), to produce lunar construction material. Analog materials (lunar regolith simulants) are used in technology development, for example to form bricks by regolith melting. One such simulant is LCATS-1, a melilite olivine nephelinite from Knippa, Texas [1]. For this study we focus on effects of different cooling rate on microstructural and thermal properties of crystallized LCATS-1. Bricks cool at different rates in their interior and exterior, which will result in different crystalline textures and mechanical properties. Furthermore, since thermal conductivity varies with temperature and crystallinity [2], there are potentially complex feedback relations between cooling and crystallization. Detailed measurements of thermal properties of materials crystallized at different rates therefore also provide important inputs to finite element thermal models of brick-forming processes.

Methods: The in situ differential scanning calorimetry (DSC) technique was used to investigate the solidification paths of LCATS-1 lunar regolith simulant. Samples were heated to 1500 °C at 30 °C/min and then cooled at different rates in PtRh pans, in a Netzsch DSC-404 F1 Pegasus. Cooling experiments on these compositions were performed under 1 bar nitrogen atmosphere. The heat flow curves as a function of temperature were recorded three times for each experiment: first with an empty pan (baseline), second with a sapphire reference material (standard), and third with the sample under investigation. Data for the three curves can be combined using the Netzsch Proteus software to calculate apparent heat capacity for each cooling rate. We use the term “apparent heat capacity” to emphasize that the signal can include contributions from latent heat contributions via melting (endothermic) and crystallization (exothermic).

Calorimetric measurements were combined with textural analysis conducted on basaltic melt cooled from liquidus to solidus conditions at rates of 5, 10, 20, 30, 40, 50, 60, 70 and 80 °C/min (Fig. 1). The recovered run products were mounted in resin and polished for microscopic analysis. In addition to reflected light microscopy, images were collected in the back-scattered electron (BSE) mode on a Zeiss Crossbeam 340 Focused Ion Beam Scanning Electron Microscope. The chemical compositions of phases were determined by qualitatively using energy dispersive spectroscopy (EDS) mapping.

Results: The major crystallizing phases were olivine, followed by pyroxene and magnetite (Figs. 1, 2).

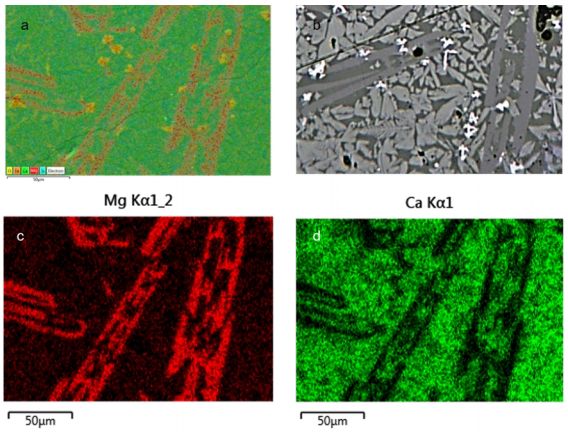

Fig.1: EDS images of LCATS-1 at 80 ˚C/min cooling rate. (a) composite (the colors yellow, orange, green and red represent O, Fe, Ca and Mg respectively). (b) BSE image (c) EDS map of Mg (skeletal olivine) (d) EDS map of Ca (pyroxene).

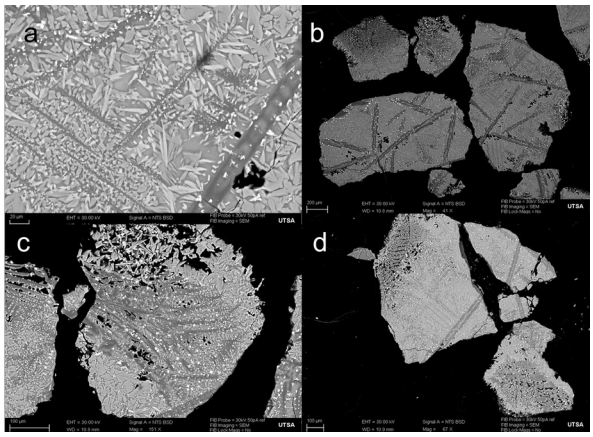

Fig.2: Back-scattered electron (BSE) images of LCATS-1 crystallized at 80 ˚C/min cooling rate. Dark grey represents skeletal olivine and light grey represent pyroxene. Bright grains are magnetite (scale bar: a: 20 µm, b: 200 µm, c and d: 100 µm).

Faster cooling results in greater undercooling and nucleation delay, so the crystallization temperature of

olivine decreases from 1298 ˚C at 5 ˚C/min to 1171 ˚C at 80 ˚C/min cooling rate (Fig. 3). Likewise, the crystallization temperature of pyroxene varies between 1100 ˚C at 5 ˚C/min to 1050˚C at 80 ˚C/min. Exothermic crystallization peaks are higher and narrower at slower cooling rates.

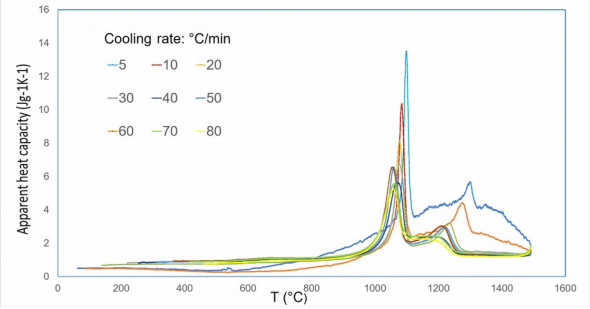

Fig. 3. Apparent heat capacity vs temperature for the LCATS-1 simulant crystallized at different cooling rates. The exothermic peaks represents crystallization of olivine, from 1300 to 1170˚C, and pyroxene, around 1100 to 1050 ˚C.

Cooling rates play a crucial role in the microstructural evolution of textures, crystal size distributions and growth rates of crystallized olivine, clinopyroxene and magnetite (Fig.4). In particular, the difference between size and shape (faceted vs. dendritic) of minerals at higher and lower crystallization rate is notable and may lead to different mechanical properties between the interiors and exteriors of bricks.

Modeled cooling histories for the interior and exterior of a 160 mm diameter brick over time are shown in Figure 5. These are finite element simulations starting from 1300 ˚C, including temperature dependent thermal properties and the enthalpy of crystallization. Cooling rates range from ~30 to ~600˚C/minute, the latter not achievable in our calorimeter.

Conclusion: Over the range of cooling rates expected to be encountered in brick production from molten regolith, crystal size decreases and crystal shapes change from faceted to dendritic. Further measurement of thermal and physical properties (texture, strength, etc.) of the experimental materials produced at different cooling rate is needed in order to optimize the brick properties and production techniques.

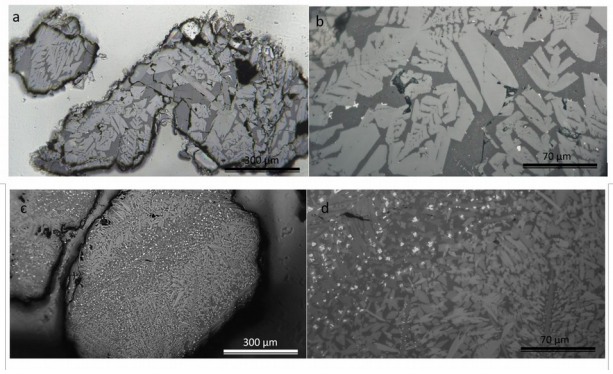

Fig. 4: Reflected light microscopic images of recovered products of LCATS-1 after crystallization at different cooling rates. (a) and (b): LCATS-1 crystallization texture at 5 ˚C/min, (c) and (d): crystallization texture at 80 ˚C/min cooling rate. Dark grey represents olivine and light grey represents pyroxene. Bright grains are magnetite. (scale bar: a and c 300 µm; b and d 70 µm).

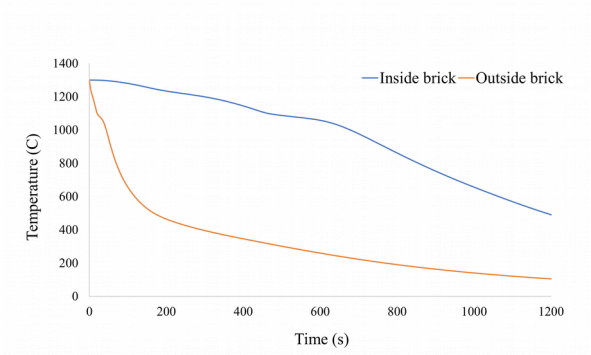

Fig. 5. Thermal modeling for LCATS-1. Internal and external temperature changes of the brick over time (both radiative and conductive cooling considered).

Acknowledgments: This research was supported by NASA contract award 80NSSC21C0406 to Astroport Space Technologies, Inc., and UTSA.

References: [1] Hooper D.M. et al. (2020) 51st LPSC abstract 2548. [2] Hofmeister A.M. et al. (2016) J Volc Geotherm Res, 327, 330-348.